Steepness effect on modulation instability of the nonlinear wave train

Wen-Son Chiang
Tainan Hydraulics Laboratory, National Cheng Kung University, Tainan 701, Taiwan

Hwung-Hweng Hwung[a)]
Department of Hydraulics and Ocean Engineering, National Cheng Kung University, Tainan 701, Taiwan

(Received 15 February 2006; accepted 20 December 2006; published online 23 January 2007)

The long-term evolution of a nonlinear wave train in deep water with varied initial wave steepness between 0.1 and 0.3 was experimentally investigated in a super wave flume (300 m long, 5 m wide, and 5.2 m deep). The initial wave train was the combination of one carrier wave and a pair of imposed sideband components which is the most unstable mode, referred to as sideband instability theory. Sixty-six wave gauges were installed downstream along the wave flume to simultaneously measure the evolution of a wave train. Increasing modulation of the wave train was observed due to sideband instability until a critical value which either wave breaking is initiated or maximum modulation is reached. The near recurrence of the initial state of the wave train is exhibited for the nonbreaking case. An effective frequency downshift of the wave spectrum accompanied with wave breaking is observed as the initial wave steepness is larger than 0.11. At postbreaking, the wave train reveals periodic modulation and demodulation, meanwhile, the related wave spectrum shows a down and upshift, respectively. Present results support the hypothesis that the frequency downshift induced by wave breaking is not permanent. © *2007 American Institute of Physics*.
[DOI: 10.1063/1.2433941]

I. INTRODUCTION

An ocean wave always exhibits modulation and deformation as it propagates. A lot of interesting and important features of nonlinear wave dynamics have been discovered. In their cornerstone paper, Benjamin and Feir[1] found experimentally and analytically that the weakly modulated Stokes wave is unstable. This result is known as "Benjamin-Feir" instability. Specifically, their analysis demonstrated that the unstable sideband components would grow exponentially with a time rate dependent on the dimensionless sideband space, $\hat{\delta}$, and initial wave steepness, ε. For weakly nonlinear and narrow-banded wave trains, the leading order complex amplitude of the modulated surface displacement satisfies the nonlinear Schrödinger equation (NLS). On the basis of the NLS equation, the evolution of a wave train is expected to have a recurrence of the initial state and the envelope of surface elevation is symmetric with respect to the peak of the wave envelope. Meanwhile, previous studies on the numerical simulation of the NLS equation have revealed that a wave field with an initial narrow band could breakdown due to energy leakage to high wave number modes resulting from violation of the narrow bandwidth constraint of the NLS equation. Lo and Mei[2] numerically solved the extended NLS equation and showed the asymmetric evolution of an initially symmetric wave train. Trulsen and Dysthe[3] added an energy dissipation mechanism into the extended NLS equation to mimic wave breaking and thus a frequency downshift is manifested in their numerical simulation. Later, they proposed the BMNLS (Ref. 4) model in which the restriction of the spectrum bandwidth was relaxed to $O(\varepsilon^{1/2})$, while the same accuracy in nonlinearity was retained. Numerical investigations[5] using BMNLS for weakly nonlinear and narrow band wave trains in deep water indicate that permanent frequency downshift is prohibited in two dimensions.

On the other hand, there were relatively few experiments available that evaluated the long time evolution of a nonlinear wave train due to the limitation of appropriate experimental facilities. Lake *et al.*[6] experimentally investigated the evolution of a nonlinear wave train and confirmed the analysis of Benjamin and Feir.[1] However, they found asymmetric growth of sideband energy and further frequency downshift to a lower sideband. Melville[7] conducted an experiment on the evolution of an initial uniform wave train in deep water. They observed a frequency downshift after wave breaking and concluded that the spectrum evolution of a nonlinear wave train due to sideband instability was not only restricted to a few discrete frequencies, but also involved a growing continuous spectrum. Tulin and Waseda[8] experimentally presented the recurrence of the initial state of a wave train and the fundamental feature of wave train evolution as predicted by other investigators using NLS, in which neither frequency downshift nor wave breaking took place. The evolution of a wave train with initial moderate wave steepness in deep water shows breaking events and frequency downshift. However, the related wave spectrum at the postbreaking stage indicates that the amplitudes of the lower sideband and original carrier wave were near equal to each other. Further evolution was not examined due to the limitation on the length of their wave flume. More recently, Hwung and Chiang[9] performed experiments on the evolution of a nonlinear wave

[a)]Author to whom correspondence should be addressed. Telephone: 886+6+2387275. Fax: 886+6+2387275. Electronic mail: hhhwung@mail.ncku.edu.tw

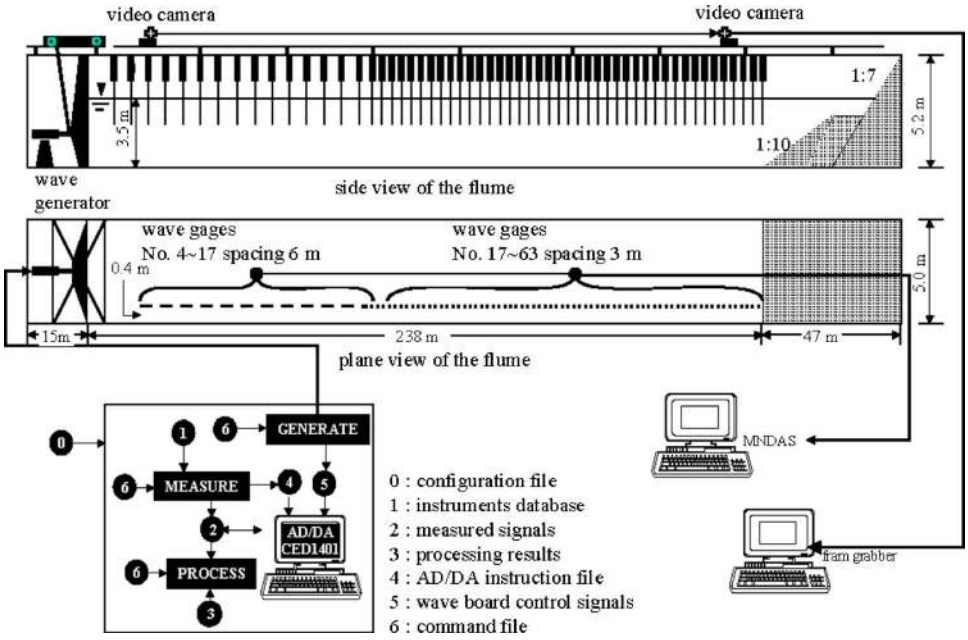

FIG. 1. Experimental setup and configuration of the wave flume.

train in a long wave flume. Extended results on the spatial evolution of wave modulation induced by sideband instability indicated that the evolution of a wave train at the postbreaking stage is a series of modulation and demodulation processes.

Herein we report our investigation into the effect of initial wave steepness on the long time evolution of a nonlinear wave train, a series of comprehensive experiments were conducted in a super wave flume in which the initial wave train is a combination of one carrier wave and a pair of sideband components. The sideband components roughly correspond to the most unstable mode referred to by Tulin and Waseda[8] and the initial wave steepness ranges from 0.1 to 0.3. The near recurrence of the initial state of a nonlinear wave train in deep water was observed when initial wave steepness was smaller than 0.11.

Selective amplification of the lower sideband occurs during the breaking process. At the postbreaking stage, the evolution of a wave train reveals a series of modulations and demodulations in which the energy of the wave train cyclically transfers between the carrier wave and sideband components. For waves with initial wave steepness less than 0.15, periodic frequency downshift and upshift were observed. On the other hand, permanent frequency downshift occurs when initial wave steepness is greater than 0.17. These results greatly extend previous studies on the evolution of sideband instability of wave trains and allow for the verification and improvement of numerical models.

In Sec. II, the experimental setup and the methodology of data analysis are described. The evolution of a wave train without breaking is introduced in Sec. III. The results for an initial modulated wave train with varied wave steepness are presented in Sec. IV. Some kinematic phenomena and dynamic behavior of wave trains are discussed. Finally, the remarkable conclusions are summarized in Sec. V.

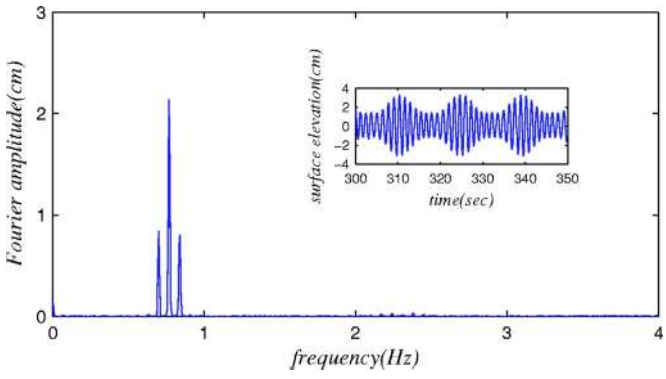

FIG. 2. The typical time series and Fourier amplitude of wave maker displacement. The given wave train is a combination of one carrier wave and two sideband components, whose wave condition is a_c=4.43 cm, T_c=1.3 s, $\hat{\delta}$=1.0, and $a_{\pm}/a_c$=0.3.

II. EXPERIMENTS AND DATA ANALYSIS

The experiments were performed in a long wave flume at Tainan Hydraulics Laboratory of Taiwan. The flume is 300 m long, 5.0 m wide, and 5.2 m deep. Figure 1 shows a schematic diagram of the experimental setup. A programmable, high resolution wave maker is located at one end of the flume and an effective wave-absorbing beach is at the opposite end. The evolution of surface wave trains is recorded using 66 capacitance-type wave gauges which are distributed 15–240 m downstream of the wave maker. The

TABLE I. The experimental conditions.

Case	T_c (s)	$\varepsilon=k_c a_c$	$k_c h$	$\hat{\delta}=\Delta\omega/(\omega_c\varepsilon)$	$a_{\pm}/a_c$
T172	1.6	0.109	5.5	0.89	0.3
T091	1.6	0.130	5.5	0.87	0.3
T164	1.3	0.129	8.3	0.87	0.3
T166	1.3	0.150	8.3	0.85	0.3
T168	1.3	0.171	8.3	0.84	0.3

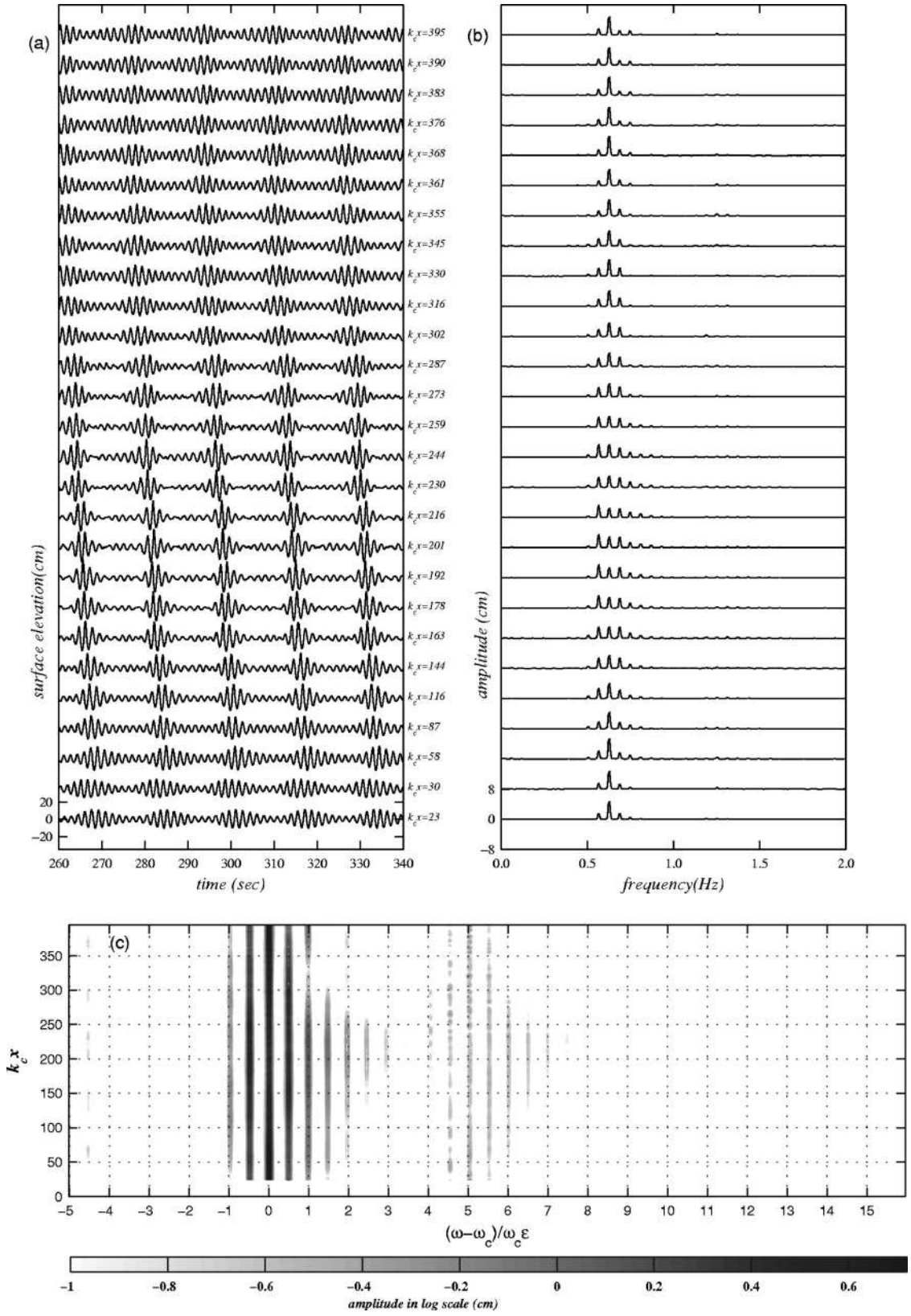

FIG. 3. (a) The measured surface elevations at several selected locations for the initial wave train case T172. The time axis is shifted according to the linear group velocity in deep water. (b) The corresponding wave Fourier amplitude. (c) The snapshot of amplitude contours plot as a function of the normalized frequency difference and fetch.

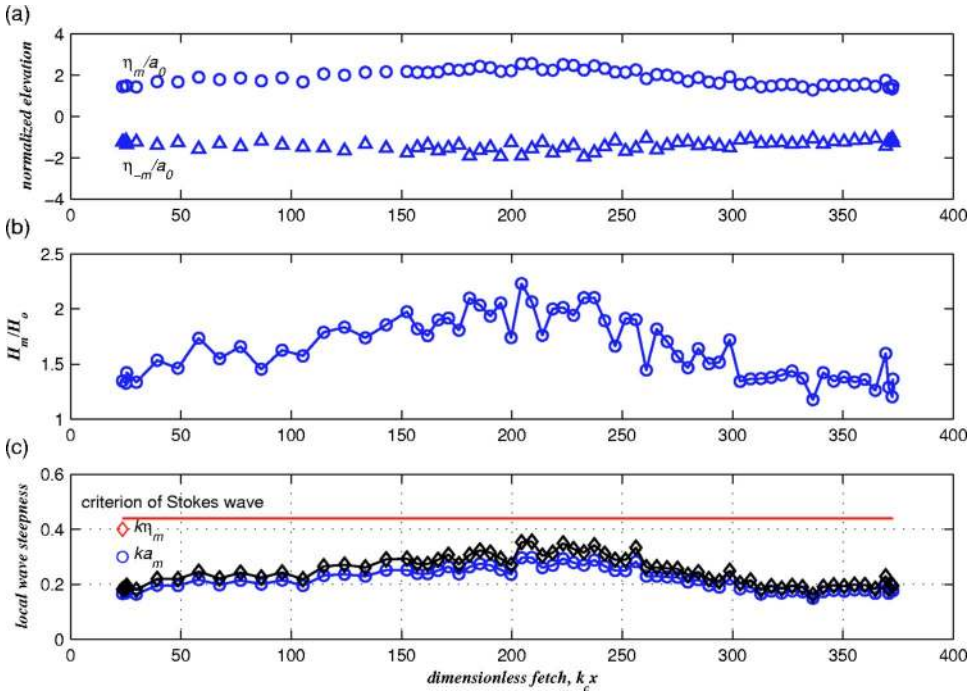

FIG. 4. Evolution of local maximum wave characteristics downstream along the fetch for case T172. (a) Normalized crest and trough elevation; (b) normalized wave height; (c) local maximum wave steepness based on maximum wave height, ka_m, and crest elevation, $k\eta_m$.

time series of water surface elevations are simultaneously acquired at a 25 Hz sampling rate and stored for further processes. Each experimental run is recorded for 10 min in real time in order to provide enough data samples for an accurate calculation of the power spectrum. The time interval between two successive measurements taken every 35 min, during which the long wave in the flume can be damped throughout. A detailed description of the experiment has been presented by Hwung and Chiang.[9]

The experiments are performed using computer-generated wave forms given by Eqs. (1a)–(1c) that are input into the wave maker servosystem. The wave forms are composed of a carrier wave of prescribed angular frequency and a pair of sideband components with a prescribed frequency difference between the carrier wave and sidebands. The imposed sidebands approximately correspond to the most unstable mode obtained according to the calculations of Tulin and Waseda.[8] The initial magnitudes of the sideband amplitudes relative to that of the carrier wave are also prescribed. A wide range of initial wave profiles are generated in the experiments by varying the initial wave steepness and the frequency differences between the carrier wave and sideband components. In order to minimize the transient wave front from initial wave generation, a ramp function is applied to the wave maker during the starting and ending of waveboard motion. A typical time series and the Fourier amplitude of wave maker displacement are shown in Fig. 2, which demonstrates that the wave maker is stable and can accurately generate the given wave form,

$$\eta(t) = a_c \sin(\omega_c t) + a_\pm \sin(\omega_\pm t + \phi_\pm), \tag{1a}$$

$$\omega_\pm = \omega_c \pm \Delta\omega, \tag{1b}$$

$$\phi_\pm = -\pi/4, \tag{1c}$$

$$a_0^2 = a_c^2 + a_+^2 + a_-^2, \tag{2}$$

where η is the free surface displacement, a_c, $a_\pm$ are amplitudes of the carrier wave and imposed sidebands, ω_c is the angular frequency of the carrier wave, $\Delta\omega$ is the frequency difference between carrier wave and imposed sidebands, x is the horizontal coordinate, and t is time. The total amplitude, a_0, is defined as Eq. (2). Initial wave steepness and the dimensionless frequency difference between the carrier wave and imposed sidebands are described in Eqs. (3) and (4). The

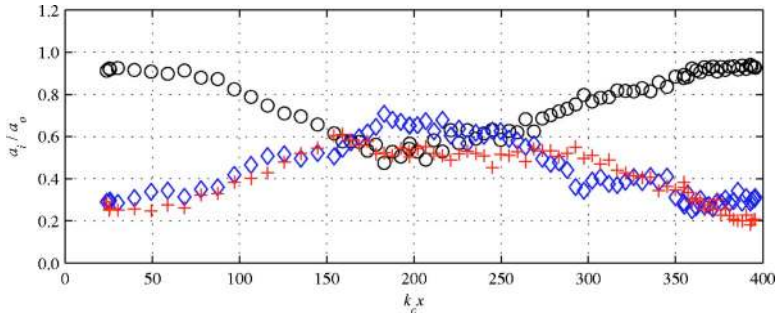

FIG. 5. The spatial evolution of dimensionless amplitudes including one carrier wave (circle) and two imposed sideband components (lower sideband: diamond; upper sideband: cross) which roughly corresponded to the most unstable mode for case T172.

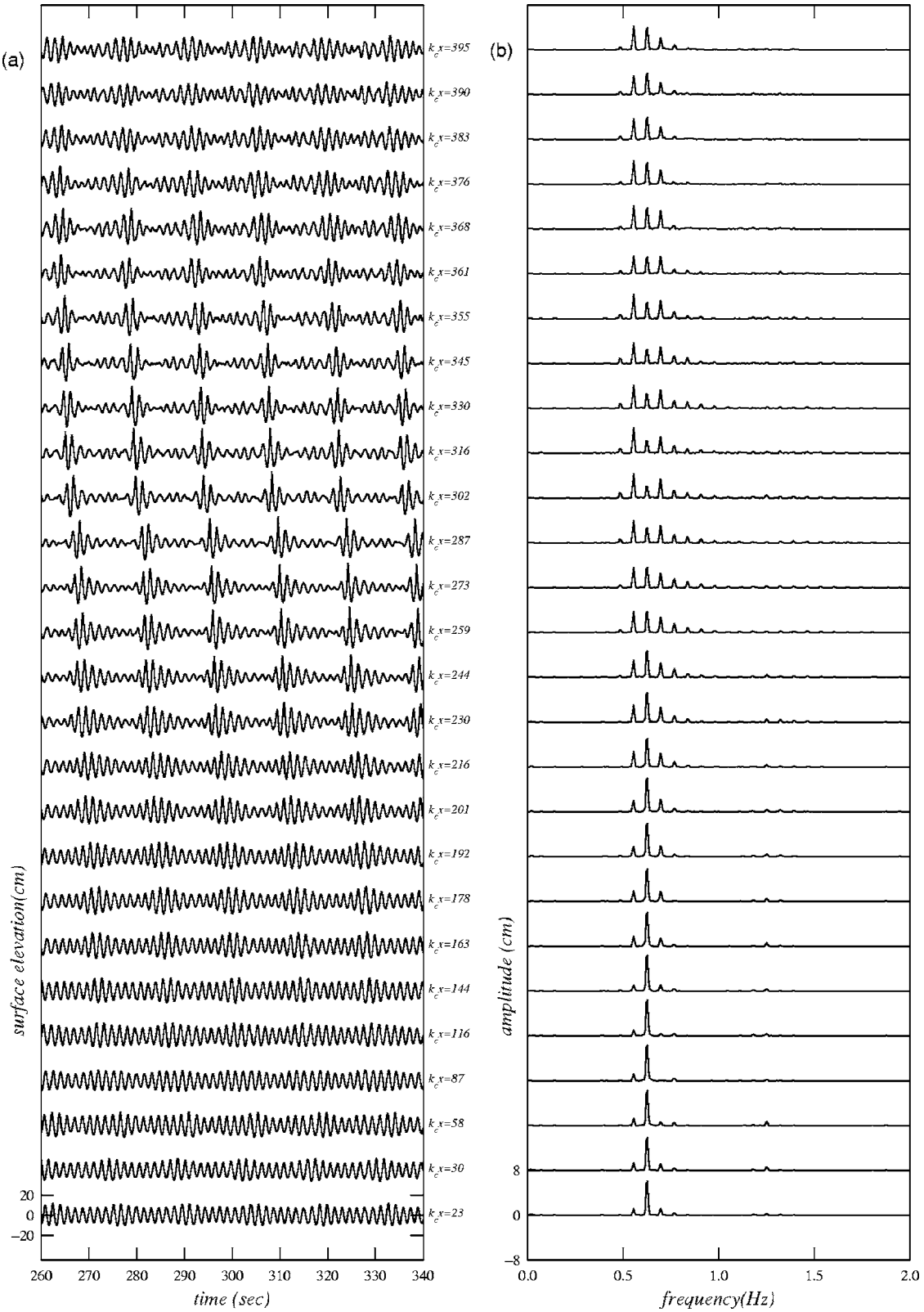

FIG. 6. (a) The measured surface elevations at several selected locations for case T091. The time axis is shifted according to the linear group velocity in deep water. (b) The corresponding wave Fourier amplitude.

stroke of the waveboard is related to the wave amplitude given by linear wave maker theory,

$$\varepsilon = k_c a_0, \tag{3}$$

$$\hat{\delta} = \Delta\omega/\omega_c\varepsilon. \tag{4}$$

Spectrum analysis is a useful method to analyze the phenomenon of wave evolution such as the analysis of the side-

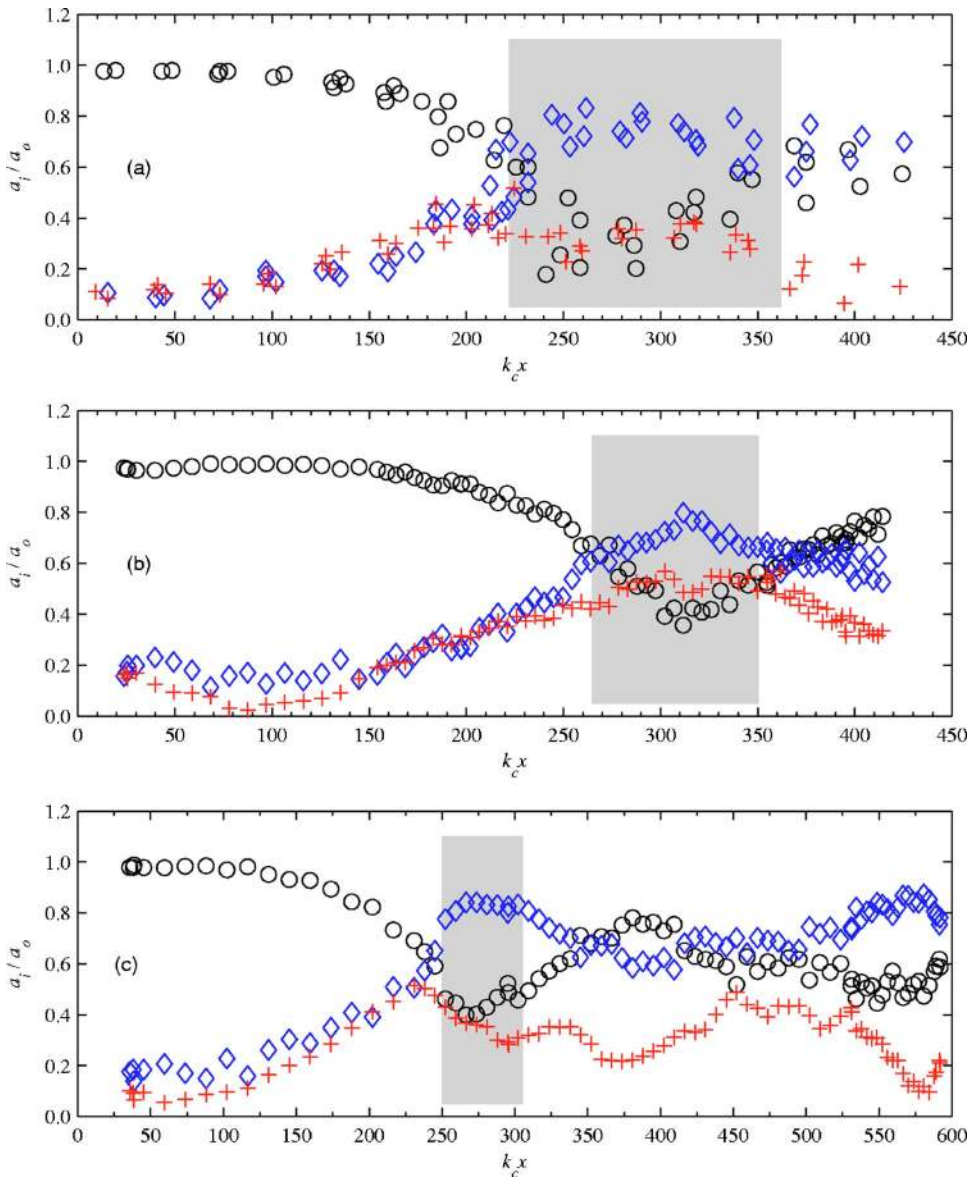

FIG. 7. The spatial evolution of dimensionless amplitudes including one carrier wave (circle) and two imposed sideband components (lower sideband: diamond; upper sideband: cross) which roughly corresponded to the most unstable mode. (a) Tulin and Waseda's (Ref. 8) Fig. 13; (b) case T091; (c) case T164. The hatch area indicates the breaking region according to the video record of the experiments.

bands energy level, the initial growth of sidebands, and the evolution of the wave spectrum. The spectrum is obtained by using a discrete Fourier transformation with the Hanning window. Specifically, the spectrum is calculated within the frequency range of 0–12.5 Hz with a resolution bandwidth of 0.006 Hz, which is much smaller than the frequency difference between the carrier wave and the initially imposed sidebands in all experimental runs. From the spectrum, the amplitudes of wave modes $(a_c, a_\pm)$ can be expressed as the square root of the total energy of the corresponding wave spectral peaks.

In addition, local maximum wave parameters of the wave train are analyzed based on the third order of Stokes wave theory combined with measured crest elevation and wave period, which is defined by the zero up-crossing method. The local wave number (k) is calculated by solving a set of coupled equations. Detailed procedures for obtaining the local wave number can be found in Grue *et al.*[10] Then, local wave steepness, ka_m and $k\eta_m$, defined as half of the wave height and crest elevation, respectively, can be estimated.

In the following sections, several typical results are discussed in great detail and the wave conditions are listed in Table I. In particular, case T172 represents a nonbreaking case. The rest of the wave trains used to examine the effects of initial wave steepness on the evolution of wave trains were all breaking cases.

III. EVOLUTION OF WAVE TRAINS WITHOUT BREAKING ($\varepsilon \cong 0.109$)

In this section, the near recurrence evolution of a nonlinear wave train is presented. The initial wave steepness, ε, is 0.109 and the relative water depth, $k_c h$, is 5.50. The spatial evolution of surface elevation and wave Fourier amplitude at several locations downstream along the wave flume and the Fourier amplitude contours as a function of fetch and normalized frequency difference are shown in Fig. 3. The initial

wave train exhibits a linear superposition of one carrier wave and two small sidebands. During the initial stage of evolution, the modulation of surface elevation exhibits a slow oscillation with an increasing trend that accompanies the symmetric growth of the imposed sideband components as shown in Fig. 3(a). As the wave train further evolves, the modulation becomes stronger and the envelope of the wave group leans forward with the corresponding energy spread over frequencies that are higher than the upper sideband. Meanwhile, asymmetric growth of the sideband amplitudes is observed in Fig. 3(b). A maximum modulation is then reached where the spectrum reveals a frequency downshift. The wave group arrives at an earlier time during the modulation increasing process which indicates an increasing group velocity due to a nonlinear effect. At a later stage, the wave train demodulates and eventually the greatest portion of the energy resides in the original three wave components. However, the earlier spreading energy is not perfectly transferred back to the original wave components which prevents full recurrence. Apart from the near recurrence, the number of waves in a group is temporarily reduced near the location of the peak modulation, where the minimum amplitude of an individual wave in a wave group approaches zero. A crest pairing process in which two waves merge is investigated near the local minimum amplitude. However, the initial number of waves in a group is recovered after a crest splitting process which is found during the later demodulation stage. This result illustrates that wave breaking is not a necessary condition in the asymmetric evolution of sidebands. In addition, the resonant nonlinear interactions which lead to the instability of nonlinear wave trains possess a reversible tendency, which can be seen by spreading energy over a high frequency during increasing modulation and then transferring most of the energy back to the original wave components in the demodulation process as shown in Figs. 3(b) and 3(c).

For an initially smaller perturbation $(a_{\pm}/a_c)$ at the same wave steepness $(\varepsilon=0.109)$, no evident growth of seeded sidebands was observed in our experiments which could be attributed to the limitation on the length of the wave flume and/or the viscous effect on the sidewall and bottom of the wave flume. Segur *et al.*[11] proved that weak dissipation plays a critical role in the stabilization of sideband instability for initial small wave steepness and perturbation. However, their prediction fails to describe the evolution of a wave train with either larger wave steepness or a large perturbation as shown in Fig. 3.

Figure 4 shows the spatial evolution of the local maximum surface elevation, wave height, and wave steepness downstream along the wave flume for a nonbreaking case (T172). The maximum amplification of wave height (H_m/H_0) is 2.23. However, the maximum value of η_m/a_0 is almost equal to 2.56. These results indicate the horizontal asymmetry of a wave profile when a transient large wave is observed. In addition, the local maximum wave steepness, ka_m and $k\eta_m$, are much lower than the geometric breaking criterion of the Stokes wave which implies that no breaking occurs. This is consistent with the visual observation of the experiment. Since most of the energy of the wave train resides in one carrier wave and a pair of sidebands during the evolution of a wave train, as shown in the Fourier amplitude, it is instructive to see how the wave energy is transferred. The spatial evolution of the dimensionless amplitudes of one carrier wave and two sidebands is evaluated and the result is shown in Fig. 5. The recurrence of the initial state of a wave train is evidently seen through a cycle of modulation and demodulation processes. However, the recurrence is not perfect due to the reason mentioned above.

IV. EVOLUTION OF WAVE TRAINS WITH BREAKING

Wave breaking is observed in strongly modulated wave trains in the present experiments when initial wave steepness is larger than 0.11. Three sets of experimental results for varied initial wave steepness are discussed in the following sections.

A. Initial wave steepness $\varepsilon \cong 0.130$

The temporal variation of surface elevation and wave Fourier amplitude at several locations downstream along the wave flume are shown in Fig. 6 for the case of initial wave steepness $\varepsilon \cong 0.130$ (T091). The modulation of a wave train increases with fetch until the strongest modulation is reached, where most of the energy of the wave train is focused into the wave group center with three energetic individual waves. The time series of surface elevation at fetch $k_c x=259$ shows a large transient wave which is much larger than the preceding and following waves. The result provides a mechanism for the generation of a freak wave resulting from sideband instability. Around this stage, wave breaking is identified on the front of the modulated wave train according to a video record of the experiment. In Fig. 6(a), the breaking phenomenon intermittently appears and lasts until fetch $k_c x=320$ in this case. During the breaking process, the lower sideband exhibits selective amplification. A frequency downshift is demonstrated at the cessation of wave breaking. Then, the wave train starts a demodulation process and the energy of the wave train transfers from the lower sideband back to the carrier wave as shown in Fig. 6(b). The amplitudes of the carrier wave and lower sideband almost coincide near the end of the wave flume. Figure 7 compares the evolution of dimensionless amplitudes of the carrier wave and two imposed sidebands for cases with almost the same initial wave steepness. For the sake of comparison, Tulin and Waseda's[8] experimental result is also shown in Fig. 7(a). Due to the limitation of flume length, they conducted a series of experiments in which sidebands of different amplitudes were imposed at the paddle. Then, the measurements were patched together to obtain the evolution in an effectively longer channel. The amplitudes of the carrier and lower sideband almost coincided near the end of their flume. The evolution of dimensionless amplitudes for case T091 is shown in Fig. 7(b), which confirms Tulin and Waseda's result. Figure 7(c) shows the spatial evolution of three imposed components with a shorter carrier wavelength and initial wave steepness $\varepsilon \cong 0.129$ (case T164). The effective fetch is therefore longer and a much more comprehensive evolution of dimensionless amplitudes is observed in this case. Moreover, a near peri-

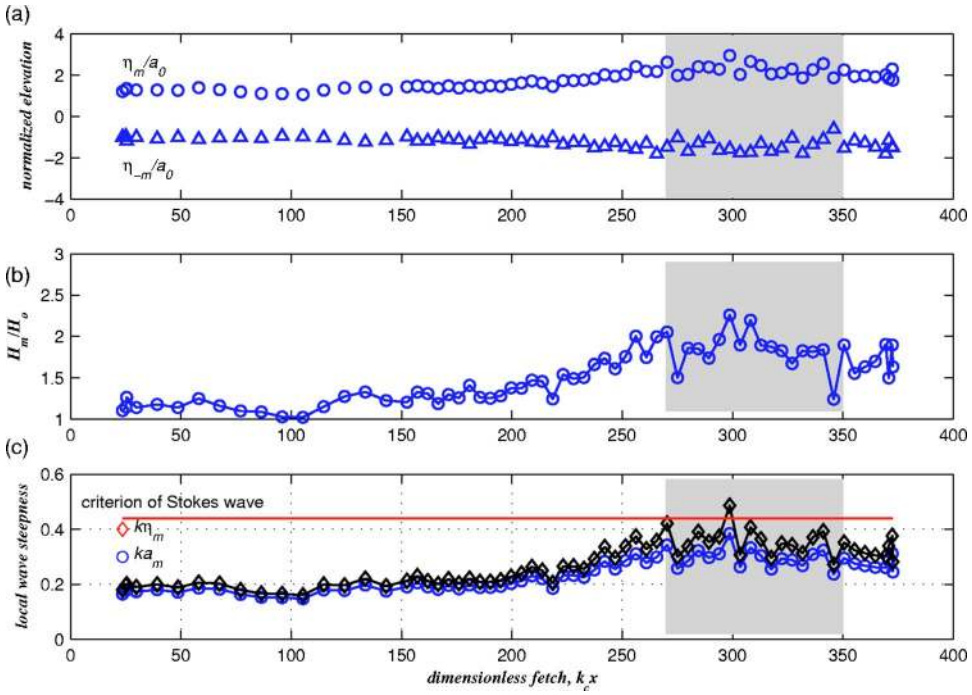

FIG. 8. Evolution of local maximum wave characteristics downstream along the fetch for case T091. (a) Normalized crest and trough elevation; (b) normalized wave height; (c) local maximum wave steepness based on maximum wave height, ka_m, and crest elevation, $k\eta_m$.

odic oscillation is found for the amplitudes of the carrier wave and the lower sideband after wave breaking. The present results largely extend previous studies on long time evolution of a nonlinear wave train. The results indicate that the frequency downshift induced by wave breaking may not be permanent. In Fig. 8, the parameters of a local maximum wave observed during the propagation of the wave train from case T091 are plotted as a function of dimensionless fetch. The maximum amplification factors of wave height and crest elevation are 2.26 and 2.95, respectively. The evolution of maximum wave steepness shows that the wave steepness based on wave height, ka_m, is much lower than the breaking criterion of the Stokes wave, when wave breaking is observed in the experiment. However, the wave steepness based on crest elevation, $k\eta_m$, approximately agrees with the breaking threshold of the Stokes wave. The analyzed local parameters at wave breaking that were observed in a strongly modulated wave train indicate that the breaking criterion of the Stokes wave is significantly inconsistent with the experimental results. Figure 9 shows the local maximum wave observed during the propagation of the wave train from case T164. The same qualitative features as case T091 are also presented.

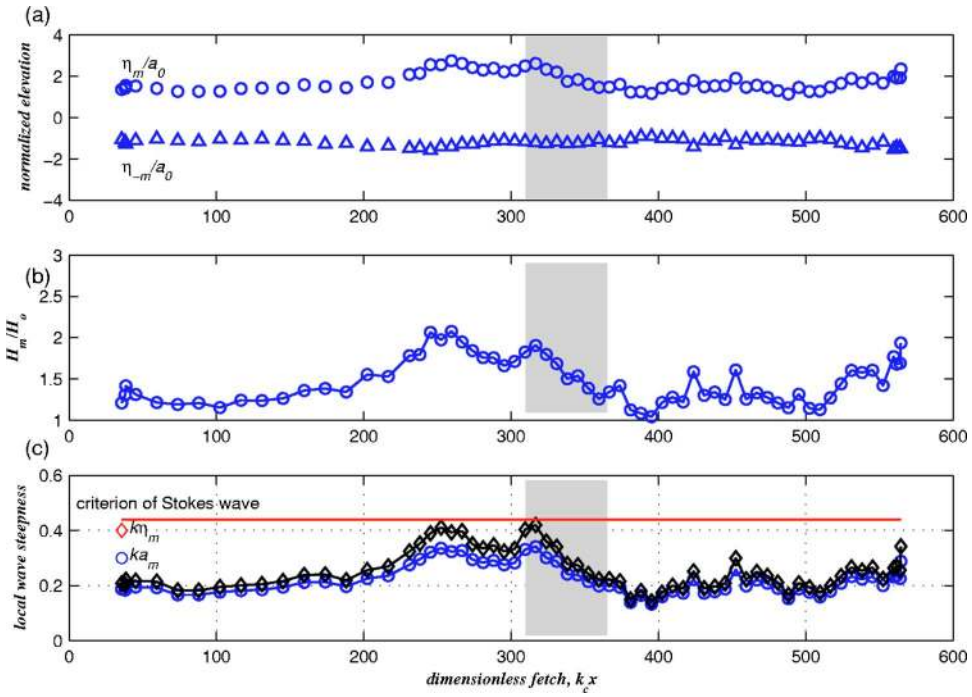

FIG. 9. Evolution of local maximum wave characteristics downstream along the fetch for case T164. (a) Normalized crest and trough elevation; (b) normalized wave height; (c) local maximum wave steepness based on maximum wave height, ka_m, and crest elevation, $k\eta_m$.

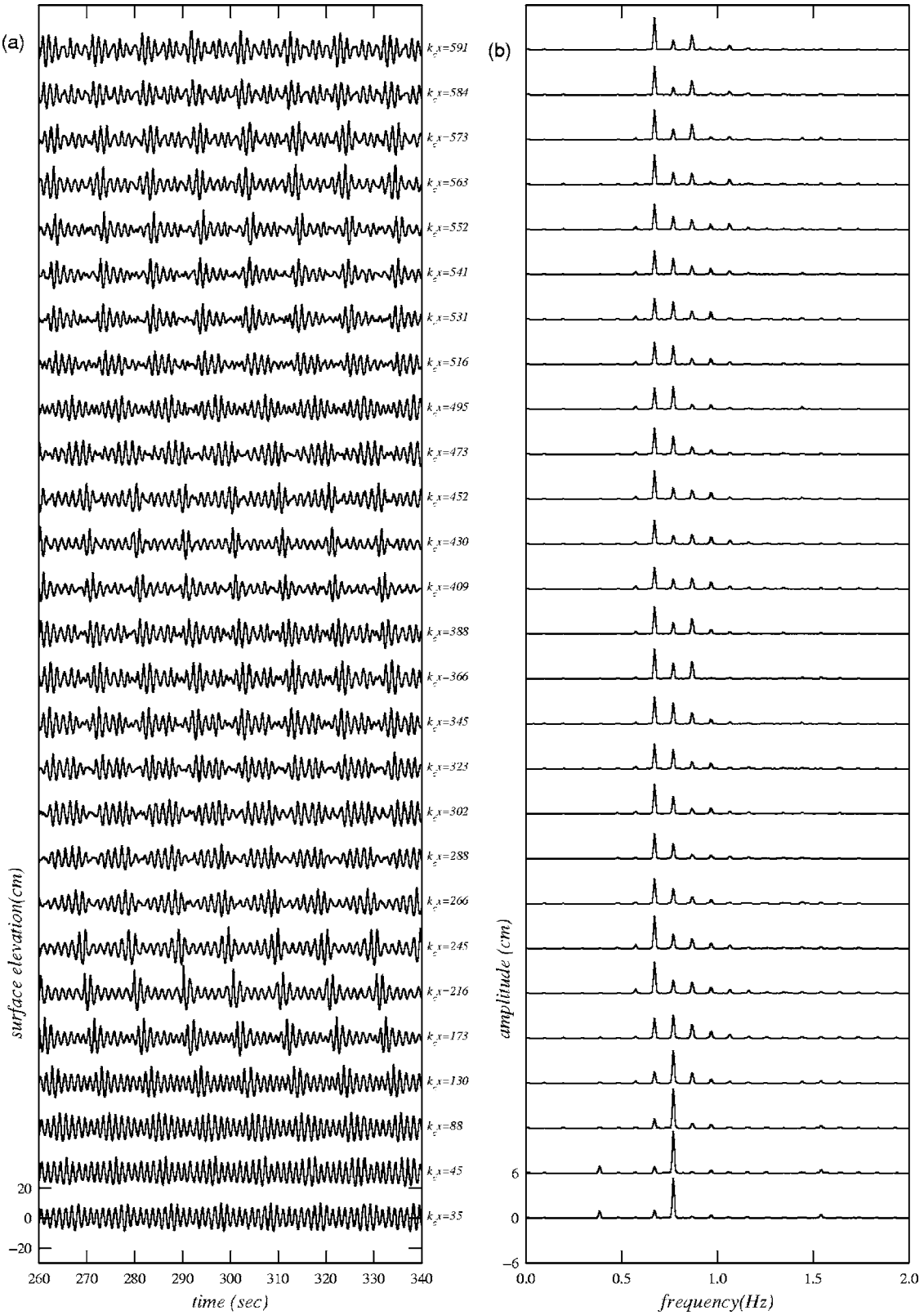

FIG. 10. (a) The measured surface elevations at several selected locations for case T166. The time axis is shifted according to the linear group velocity in deep water. (b) The corresponding wave Fourier amplitude.

B. Initial wave steepness $\varepsilon \cong 0.150$

The evolution of a wave train with initial steepness $\varepsilon = 0.150$ (case T166) is exhibited in Fig. 10, for which the surface elevation and the corresponding wave Fourier amplitude are shown at several gauge stations. Comparison between the modulations of wave trains with $\varepsilon = 0.130$ and $\varepsilon = 0.150$ shows that the evolution of a wave train accelerates as initial wave steepness increases. Therefore, wave breaking

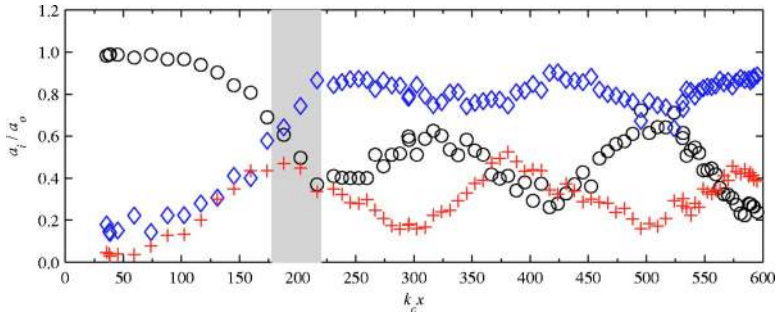

FIG. 11. The spatial evolution of dimensionless amplitudes including one carrier wave (circle) and two imposed sideband components (lower sideband: diamond; upper sideband: cross) which roughly corresponded to the most unstable mode for case T166.

occurs earlier for wave trains with larger initial wave steepness. Evidently, the wave train periodically exhibits modulation and demodulation at the postbreaking stage. At this stage, most of the energy of the wave train transfers between the carrier wave and a pair of sidebands as shown in Fig. 11. The amplitude of the lower sideband increases as the modulation of the wave train increases. In contrast, the amplitude of the carrier wave increases during the demodulation process. The comparison between Fig. 7(c) and Fig. 11 indicates that the amount of energy transfer between the wave components at the postbreaking stage is less active for a wave train with $\varepsilon=0.150$ than for a wave train with $\varepsilon=0.130$. More specifically, the energy recovery rate of a carrier wave decreases as initial wave steepness increases. So, a permanent frequency downshift is observed for a wave train with $\varepsilon=0.150$. However, a temporary frequency downshift is found for a wave train with $\varepsilon=0.130$. The local parameters for maximum waves as observed at gauge stations for wave trains with $\varepsilon=0.150$ are given in Fig. 12. The maximum amplification factors of wave height and crest elevation are 1.81 and 2.43, respectively, which are smaller than those of wave trains with $\varepsilon=0.130$. Meanwhile, the local wave steepness attains a maximum value of 0.45 at fetch $k_c x=188$, where wave breaking is initiated.

C. Initial wave steepness $\varepsilon\cong 0.171$

As initial wave steepness further increases, the transient large wave is observed earlier. Experimental results of a wave train with $\varepsilon=0.171$ (case T168) are shown in Figs. 13–15. The maximum amplification factors of wave height and crest elevation are 1.74 and 2.22. The dimensionless amplitude of lower sideband remains almost constant with very little oscillation. An effective frequency downshift is found after wave breaking. Although it was not shown here, the consistent trend of the evolution of dimensionless amplitudes of one carrier wave and two sidebands are confirmed for even larger initial wave steepness. Wave breaking is observed when the local wave steepness based on crest elevation is larger than 0.44 or, equivalently, when the corresponding ratio of horizontal velocity at wave crest to the phase velocity is larger than 0.5. These results are quite consistent in our experiments.

In summary, the evolution of wave trains accelerates as the initial wave steepness increases. After that, the local maximum amplitude of the lower sideband component which corresponds to the cessation of wave breaking is observed earlier for wave trains with larger initial wave steepness. After the cessation of wave breaking, the wave train de-

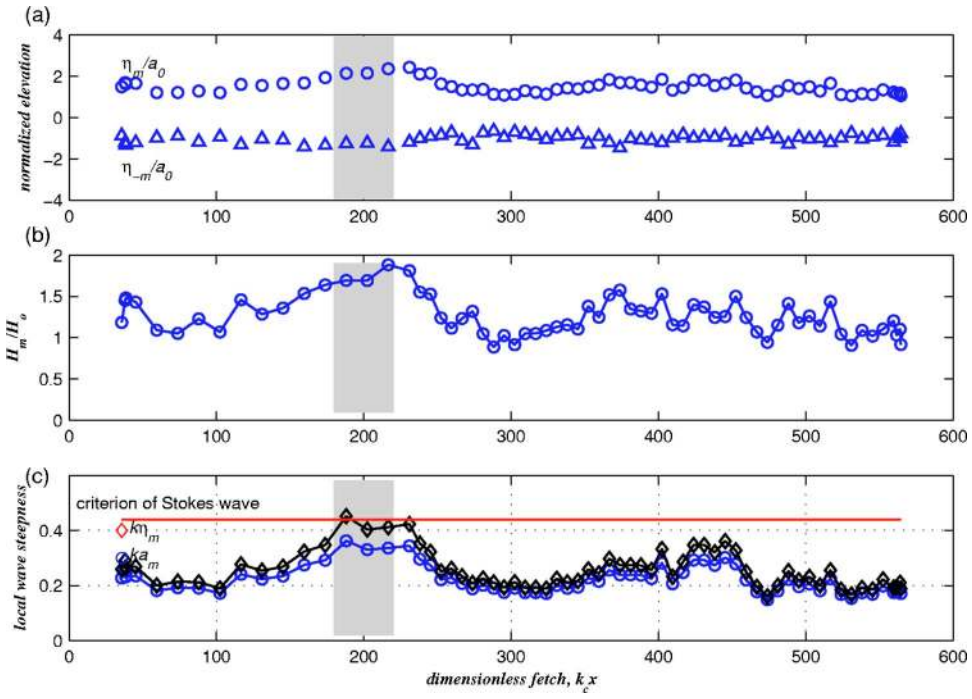

FIG. 12. Evolution of local maximum wave characteristics downstream along the fetch for case T166. (a) Normalized crest and trough elevation; (b) normalized wave height; (c) local maximum wave steepness based on maximum wave height, ka_m, and crest elevation, $k\eta_m$.

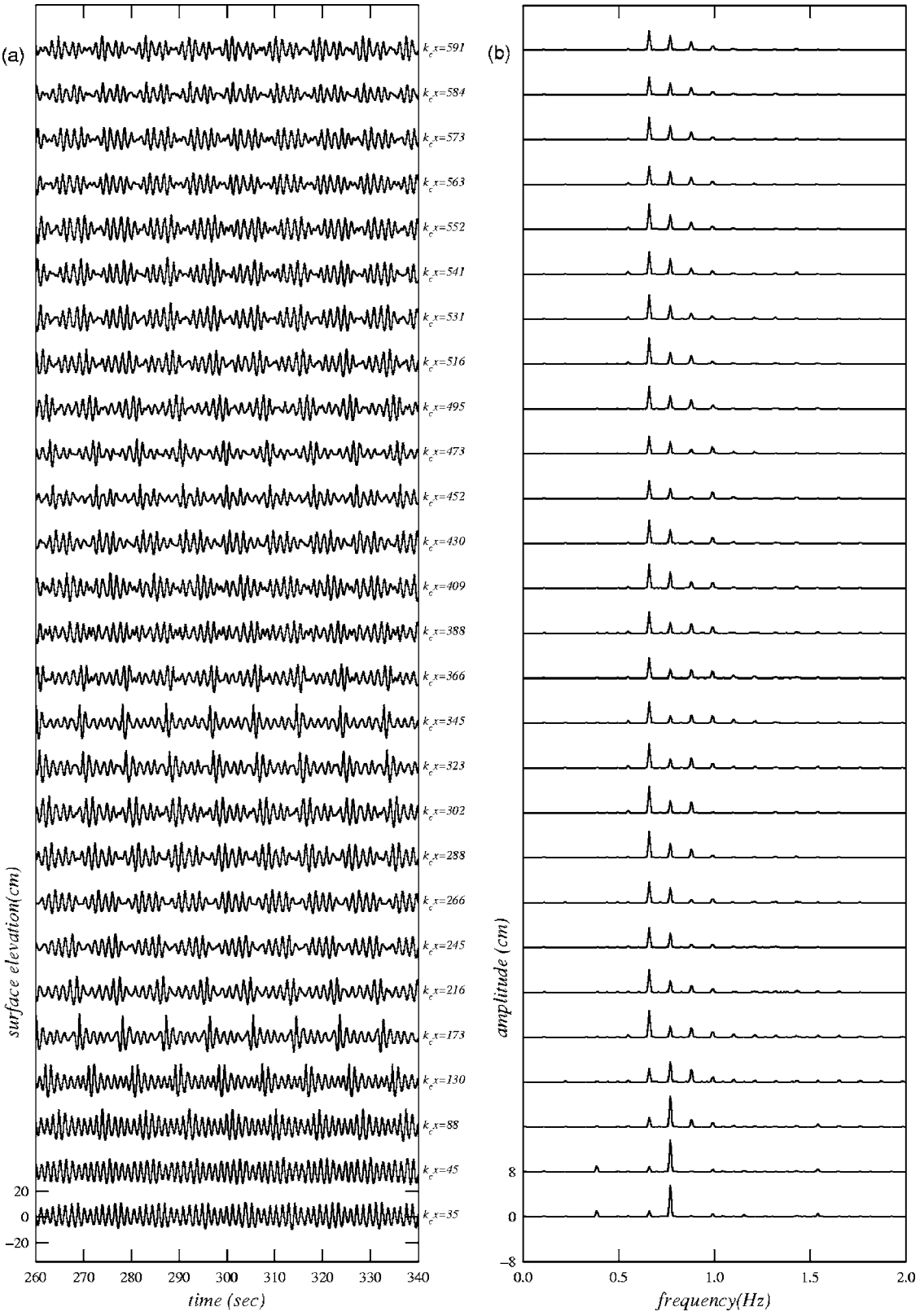

FIG. 13. (a) The measured surface elevations at several selected locations for case T168. The time axis is shifted according to the linear group velocity in deep water. (b) The corresponding wave Fourier amplitude.

modulates and the carrier wave gradually recovers its amplitude, which is accompanied by a decrease in the energy of the higher frequency and imposed sideband components. The rate of energy recovery of the carrier wave decreases as the initial wave steepness increases. For wave trains with initial wave steepness less than 0.15, the demodulation process continues until the carrier wave becomes the dominant component again, which means that the frequency upshifts to the

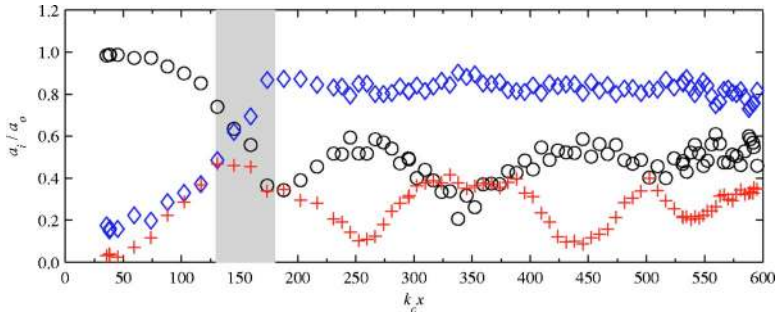

FIG. 14. The spatial evolution of dimensionless amplitudes including one carrier wave (circle) and two imposed sideband components (lower sideband: diamond; upper sideband: cross) which roughly corresponded to the most unstable mode for case T168.

original carrier wave. Therefore, the frequency downshift that was observed earlier is a temporary process. For relatively larger initial wave steepness, such as 0.17, the recovered amplitude of the original carrier wave is not strong enough to form a frequency upshift and thus permanent downshifting is observed. These results suggest that a previously recognized frequency downshift induced by wave breaking is not permanent.

The initiation of wave breaking in a strongly modulated wave train is related to the asymmetrical growth of sidebands. In addition, the local wave steepness, $k\eta_m$, at wave breaking roughly approaches the geometric criterion of the Stokes wave. Further detailed investigation is necessary to examine the breaking criterion for a modulated deep water wave train.

A wave group propagates faster with increasing modulation. This was observed in the experiments which demonstrated the correction of group velocity for the nonlinear effect. Chiang *et al.*[12] estimated the group velocity of a modulated wave train and compared the results to linear group velocity. The difference between the estimated and linear group velocity was shown for varied initial wave steepness. The estimated group velocity was nearly 10% faster than the linear group velocity.

V. CONCLUSIONS

The systematic experimental studies on the long time evolution of the nonlinear wave train were conducted in a long flume and the results are reported in this paper. The present results greatly extend previous studies on the evolution of a nonlinear unstable wave train. In particular, the effects of initial wave steepness on wave modulation are investigated in great detail. The remarkable results are summarized in the following:

(1) For initial wave steepness less than 0.11, the recurrence of the initial state of a wave train is observed which demonstrates that the spreading of energy over high frequencies during the propagation of a wave train is not an irreversible process.
(2) The initiation of asymmetric development of sideband amplitudes after initially exponential growth roughly

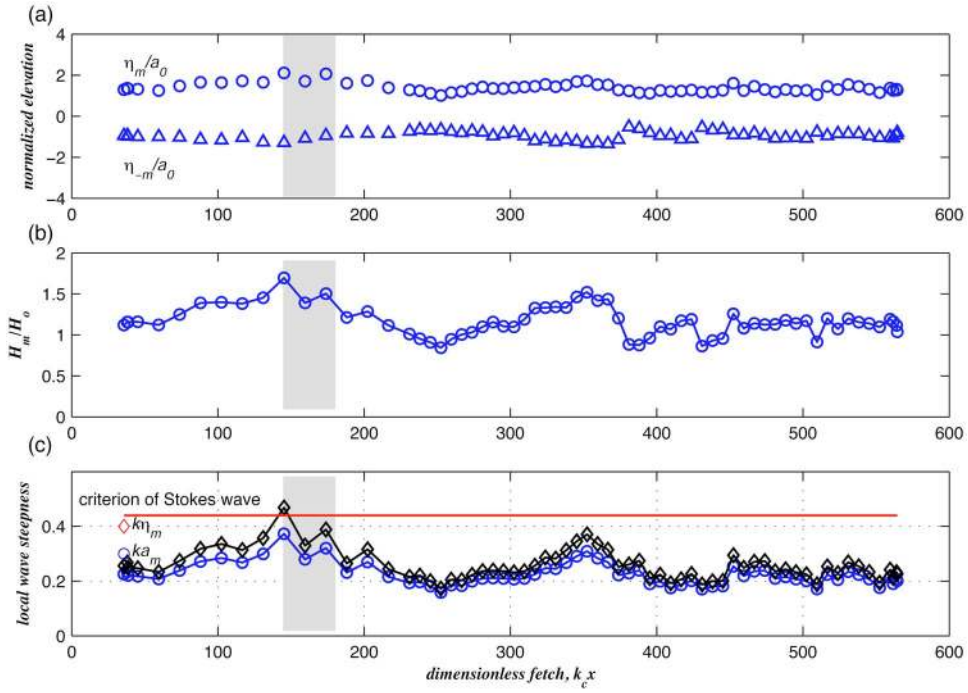

FIG. 15. Evolution of local maximum wave characteristics downstream along the fetch for case T168. (a) Normalized crest and trough elevation; (b) normalized wave height; (c) local maximum wave steepness based on maximum wave height, ka_m, and crest elevation, $k\eta_m$.

corresponds to the onset of wave breaking on a strongly modulated wave train. Melville[7] found a similar result in his experiment which was conducted in a smaller wave flume.

(3) An effective frequency downshift is found at the stage of cessation of wave breaking. At a further stage, the evolution of wave trains reveals a periodic modulation and demodulation in which most of the energy interchange of the wave train takes place between the carrier wave and two imposed sidebands. The amplitude of the carrier wave increases as the modulation increases. In contrast, the amplitude of the lower sideband increases during the demodulation process. The evolution of normalized amplitudes of the carrier wave and two sidebands demonstrates a provisional frequency downshift for moderate initial steepness and permanent frequency downshift for large initial steepness.

(4) The experimental results of our analysis of modulated wave trains indicate that local wave steepness, defined based on the local wave number and crest elevation, $k\eta_m$, at wave breaking roughly approaches the geometric criterion of the Stokes wave. Further detailed investigation is necessary to examine the breaking criterion in a modulated deep water wave train.

ACKNOWLEDGMENTS

The authors gratefully acknowledge funding from the Ministry of Education, Taiwan, Grant No. A-91-E-FA09-7-3. The authors thank Y-H. Chang and S-H. Chen for their assistance in preparing and conducting the experiments.

[1] T. B. Benjamin and J. E. Feir, "The disintegration of wave trains on deep water. Part 1. Theory," J. Fluid Mech. **27**, 417 (1967).
[2] E. Lo and C. C. Mei, "A numerical study of water-wave modulation based on a higher-order nonlinear Schrödinger equation," J. Fluid Mech. **150**, 395 (1985).
[3] K. Trulsen and K. B. Dysthe, "Frequency downshift through self-modulation and breaking," in *Water Wave Kinematics*, edited by A. Torum (Kluwer Academic, Norwell, 1990),
[4] K. Trulsen and K. B. Dysthe, "A modified nonlinear Schrödinger equation for broader bandwidth gravity waves on deep water," Wave Motion **24**, 281 (1996).
[5] K. Trulsen and K. B. Dyethe, "Frequency downshift in three-dimensional wave trains in a deep basin," J. Fluid Mech. **352**, 359 (1997).
[6] B. M. Lake, H. C. Yuen, H. Rungaldier, and W. E. Ferguson, "Nonlinear deep-water waves: theory and experiment. Part 2. Evolution of a continuous train," J. Fluid Mech. **83**, 49 (1977).
[7] W. K. Melville, "The instability and breaking of deep-water waves," J. Fluid Mech. **115**, 165 (1982).
[8] M. P. Tulin and T. Waseda, "Laboratory observations of wave group evolution, including breaking effects," J. Fluid Mech. **378**, 197 (1999).
[9] H. H. Hwung and W. S. Chiang, "Measurements of wave modulation and breaking," Meas. Sci. Technol. **16**, 1921 (2005).
[10] J. Grue, D. Clamond, M. Huseby, and A. Jensen, "Kinematics of extreme waves in deep water," Appl. Ocean. Res. **25**, 355 (2003).
[11] H. Segur, D. Henderson, J. Carter, J. Hammack, C-M Li, D. Pheiff, and K. Socha, "Stabilizing the Benjamin-Feir instability," J. Fluid Mech. **539**, 229 (2005).
[12] W. S. Chiang, H. H. Hwung, and Y. H. Chang, "Experiment on the front of continuous wavetrains in a large wave tank," in *Proceedings of the 29th International Conference on Coastal Engineering*, edited by J. M. Smith (World Scientific, Singapore, 2004).